www.ptcer.pl/mccm

MATERIAŁY CERAMICZNE /CERAMIC MATERIALS/, 62, 3, (2010), 328-334

Manufacturing and Properties of Ceramics Originated from Zirconia-Ceria Nanopowders Doped with Yttria

Waldemar Pyda*, Anna Marchlewska, Mirosław M. Bućko, Anna Pyda

AGH - University of Science and Technology, Faculty of Materials Science and Ceramics, Kraków, Poland
*e-mail: pyda@agh.edu.pl

Abstract

Ceria-zirconia nanopowders doped with yttrium(III) oxide were prepared by a soft chemistry route. A concentration of ceria in the 8 mol% yttria-zirconia nanopowder changed from 0 to 100 %. In the route, a water solution of zirconium(IV) oxychloride, yttrium(III) chloride and cerium(III) nitrate was treated with ammonia to co-precipitate a deposit, which was calcined for 2 h at 900°C in air to obtain crystalline nanopowder. Consolidation of the nanopowders was performed by means of cold isostatic pressing under 220 MPa and natural sintering for 2 h at 1550°C in air.

The effects of the ceria concentration on properties of both yttria-zirconia-ceria nanopowders and bulk materials were investigated by TG-DTA, XRD, BET, SEM and Vickers' indentation. The thermal behaviour of co-precipitated materials, crystal structure and crystallite size of the nanopowders, evolution of the microstructure and mechanical properties of the bulk materials were found to depend on ceria concentration.

Keywords: CeO_2, ZrO_2, Microstructure final, Mechanical properties, Nanopowder

WYTWARZANIE I WŁAŚCIWOŚCI CERAMIKI OTRZYMANEJ Z NANOPROSZKÓW CYRKONIOWO-CERIOWYCH DOMIESZKOWANYCH TLENKIEM ITRU(III)

Nanoproszki cero-cyrkoniowe domieszkowane tlenkiem itru(III) wytworzono za pomocą metody chemii miękkiej. Stężenie CeO_2 w nanoproszku 8 % mol. Y_2O_3-ZrO_2 zmieniało się od 0 do 100 %. W zastosowanej metodzie preparatyki, wody roztwór tlenochlorku cyrkonu(IV), chlorku itru(III) i azotanu ceru(III) zadawano wodnym roztworem amoniaku, aby współstrącić osad, który kalcynowano przez 2 h w 900°C w powietrzu, w celu uzyskania krystalicznego nanoproszku. Konsolidację nanoproszków przeprowadzono drogą prasowania izostatycznego na zimno przy ciśnieniu 220 MPa i następczego spiekania swobodnego przez 2 h w 1550°C w powietrzu.

Wpływy stężenia CeO_2 na właściwości zarówno nanoproszków w badanym układzie Y_2O_3-ZrO_2-CeO_2, jak i spieczonych materiałów zbadano za pomocą metod TG-DTA, XRD, BET, SEM oraz nakłuwania wgłębnikiem Vickersa. Stwierdzono, że zachowanie podczas obróbki cieplnej współstrąconych osadów, struktura krystaliczna i rozmiar krystalitów nanoproszków, ewolucja mikrostruktury i właściwości mechanicznych spieczonych materiał zależą od stężenia tlenku ceru(III).

Słowa kluczowe: CeO_2, ZrO_2, mikrostruktura finalna, właściwości mechaniczne, nanoproszek

1. Introduction

Ceria-zirconia solid solutions have attracted a great deal of attention due to their interesting catalytic activity and mixed conductivity. The CeO_2-ZrO_2 solid solutions have been used as an active component in the three-way catalysts (oxidation of CO and hydrocarbons and reduction of NO_x) for automotive exhaust [1]. The CeO_2-ZrO_2-$YO_{1.5}$ solid solution is a promising material for oxygen permeable membranes, which can be applied to electro-catalytic reactors or oxygen gas separators [2]. The studies of the temperature and oxygen partial pressure dependence of total and ionic conductivity showed lower ionic conductivity of the ZrO_2-CeO_2-$YO_{1.5}$ solid solutions when compared to yttria cubic-stabilised zirconia (YSZ) or yttria doped ceria (YDC) [2-5]. Therefore, the ZrO_2-CeO_2-$YO_{1.5}$ solid solution is not preferable as an electrolyte in solid oxide fuel cells (SOFCs). However, the mixed electronic and ionic conductivity of this material may make it suitable for application as electrodes, or for modification of electrolyte surfaces in the medium-temperature SOFCs.

The ZrO_2-CeO_2-$YO_{1.5}$ solid solutions are also used in the experimental investigations concerning the application of yttria cubic-stabilised zirconia (YSZ) both as an inert matrix for burning excess plutonium from spent fuels in light water reactors and as a material for nuclear waste utilization, which immobilizes actinides [6]. Cerium is traditionally used as a surrogate of tetravalent actinides, for example, plutonium.

Ceria-zirconia solid solutions are usually synthesized by the conventional ceramic techniques or co-precipitation method followed by calcination and milling. The latter method is sufficiently simple and dust free technology. The processes of co-precipitation and calcination were investigated in detail for the ZrO_2-CeO_2 solid solutions by several researchers [6-8].

Nanostructured $Ce_{1-x}Zr_xO_2$ solid solutions were synthesized by a single step solution combustion process using cerous nitrite, zirconyl nitrite and the fuel redox mixture of oxalyl dihydrazide (ODH) and carbohydrazide (CH) [9]. The method delivered powders composed of nanocrystallites, which had the sizes of 6-11 nm.

Hydrothermal method has been also employed to synthesize CeO_2 and $Ce_{1-x}M_xO_{2-\delta}$ (M = Zr, Ti, Pr, Y, Sm, Gd, Fe) using NH_{3aq} and NaOH as co-precipitating agents [10-12] or diethylenetriamine (DETA) and melamine as complexing agents [13]. Singh *et al*. reported that even up to 50 % Zr and Y, 40 % Ti, 25 % Pr or 15 % Fe was substituted for Ce^{4+} in CeO_2 by the hydrothermal method to produce the crystallites having cubic fluorite structure and the sizes ranging from 5 to 10 nm. Sizes of crystallites depended on the complexing agent and reaction temperature. Nanocrystalline CeO_2 and $Ce_{1-x}Zr_xO_2$ had improved oxygen storage capacity (OSC).

In the present work, nanopowders in the ceria-zirconia-yttria system are manufactured by the co-precipitation method and polycrystalline materials are consolidated by natural sintering. A concentration of CeO_2 in the 8 mol% yttria-zirconia solid solution changes from 0 to 100 %. The effects of the ceria addition on the thermal behaviour of co-precipitated materials, their crystal structure and morphology, evolution of the microstructure and mechanical properties of the bulk materials are studied.

2. Experimental

Zirconia-ceria-yttria powders were studied with a theoretical composition of $Y_{0.148}(Zr_{1-x}Ce_x)_{0.852}O_{2-\delta}$, where x = 0, 0.1, 0.3, 0.5, 0.7, 0.9 and 1.0. A co-precipitation method followed by calcination was used to prepare the powders as shown in Fig. 1. The following reagents were used: $ZrOCl_2{\cdot}8H_2O$ (99.7 %, Beijing Chemicals Import & Export Corporation, reagent purity), $Ce(NO_3)_3$ (86.8 % and La – 11.6 %, Nd - 0.7%, Gd – 0.9 %, UMCS, WChN Lublin), Y_2O_3 (99.99 %) and reagent grade HCl and NH_{3aq}. For manufacturing the powder, the water solution of yttrium(III) chloride, zirconium(IV) oxychloride and cerium(III) nitrite was dropwise added to vigorously stirred ammonia (1:1) in order to co-precipitate yttria-zirconia-ceria deposit at a final pH of 9.5. The deposit was washed with 0.3 % water solution of NH_4NO_3 at pH 9.5 to remove soluble co-precipitation products by using decantation and vacuum filtration. Washing the deposits was proceeded to obtain no visible reaction of filtrate with $AgNO_3$, and then the deposits were dried at 95°C to the constant weight. The deposits were comminuted to a particle size of < 550 μm by using an alumina mortar. Crystallization was performed for 2 h at 900°C in air by calcination. A heating rate of 5°/min was used. The calcined powders were attrition milled for 2 h in 2-propanol. 3Y-TZP grinding media of 2 mm in diameter were used. Green compacts of ~13 mm in diameter and ~2 mm in height were cold isostaticaly pressed under 220 MPa, using the powders added with 3 % of oleic emulsion as lubricant. The compacts were naturally sintered for 2 h at 1550°C in air. The samples were heated to 500°C with a rate of 3°C/min, and then up to maximum temperature with 5°C/min.

The thermal behaviour of the yttria-zirconia-ceria deposits was investigated by using the thermogravimetric-differential thermal analysis (TG-DTA; Derivatograph C, MOM) at a heating rate of 10°C/min under air atmosphere. The TG/DTA experiments were conducted in platinum crucibles, using the 100 mg samples and α-Al_2O_3 powder working as reference material.

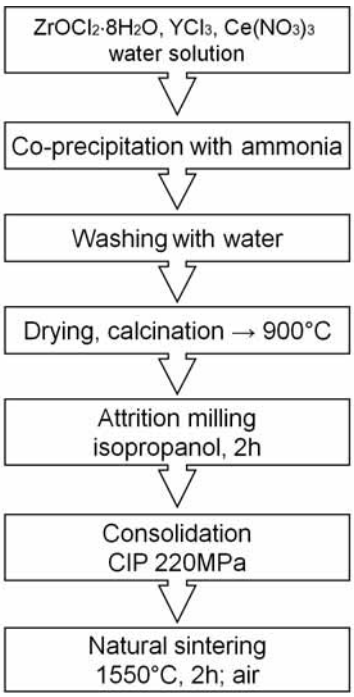

Fig. 1. Flow chart of preparation route of the zirconia-ceria-yttria powders.

The phase composition of the calcined powders and sintered materials were characterized by means of X-ray diffractometry (XRD). The X'Pert Plus apparatus (PANalytical), equipped with a lamp with copper anode, a Johansson monochromator and the X'Celerator type strip detector, was used. Counts were made in a range of 10-90°2Θ with a step size of 0.00816°, applying a continuous scan type. Rietveld refinement with X-ray diffraction data [14] by the X'Pert software was helpful to determine both the phase composition and unit cell parameters. Crystallite size in the direction perpendicular to the (111) plane was determined for the calcined powders from X-ray line broadening using the Sherrer approach [15]. Specific surface area of the powders was measured by nitrogen adsorption (BET, Nova 1200e, Quantachrome Instruments). The microstructure of the sintered polycrystals was observed on the polished and thermally etched surfaces by means of a scanning electron microscope (NOVA NanoSEM, FEI Company). Densification of the compacts was characterised by the geometrical density. Relative density of the sintered samples was determined by the Archimedes' method. Vickers' indentation under 49.03 N for 10 s in a hardness tester FV-700 (Future Tech) was applied to measure hardness and critical stress intensity factor, K_{Ic}. The Palmqvist crack model was applied for the K_{Ic} calculations [16].

3. Results and discussion

3.1. Nanopowders

The effect of the ceria addition on the thermal behaviour of yttria-zirconia hydrogels is shown in Fig. 2.

The 8YSZ hydrogel, corresponding to the 8 mol% Y_2O_3-ZrO_2 powder, was characterised by significant (11.8 %) mass loss during heating from 25 to 600°C (Fig. 2b). From 25 to 380°C, the mass loss was accompanied by a heat consumption and appearance of a broad endothermic effect (Fig. 2a), which corresponds to evolving the adsorbed gases, adsorbed and hydrated water and gases originated from the decomposition of ammonium nitrite (276°C) and other impurities. A sharp exothermic effect was detected at 434°C, which corresponds to the phase transition of the hydrogel from the amorphous to crystalline state [17-20]. No exothermal effects appeared at temperatures higher than 600°C. During heating from 600 to 1000°C, the mass of the sample continued to decrease but the mass loss was negligible (0.2 %). This can be related to the removal of the residual OH^- groups from the material structure [19].

In the case of 8 mol% yttria-ceria powder (Fig. 2b), a significant mass loss (9.8 %) is observed during heating from 25 to 1000°C and accompanied by heat consumption. The mass loss corresponds to the removal of adsorbed gases, adsorbed and hydrated water and impurities in the temperature range from 25 to 300°C, and to the elimination of the OH^- groups from the material heated above 300°C, as it was reported in the literature [6]. The DTA curve does not show any particular exothermal effect.

The thermal behaviour of the studied 8YSZ-CeO_2 powders was found to strongly depend on the ceria concentration in the material (Fig. 2). The powder containing 10 mol% ceria shows the behaviour during heating similar to the 8YSZ powder. Only the total mass loss is increased (19.2 %).

For ceria concentrations higher than 30 %, the TG-DTA curves of the powders are similar to those obtained for pure ceria. No exothermic effects are observed on the DTA curves between 500 and 1000°C. For the range of ceria concentrations higher than 30 %, the temperatures of endothermic effects varied with the ceria content. For ceria concentrations from 50 to 90 %, the temperatures of the first and second endothermic effect decrease from 125 to 86°C and from 455 to 389°C, respectively. The endothermic

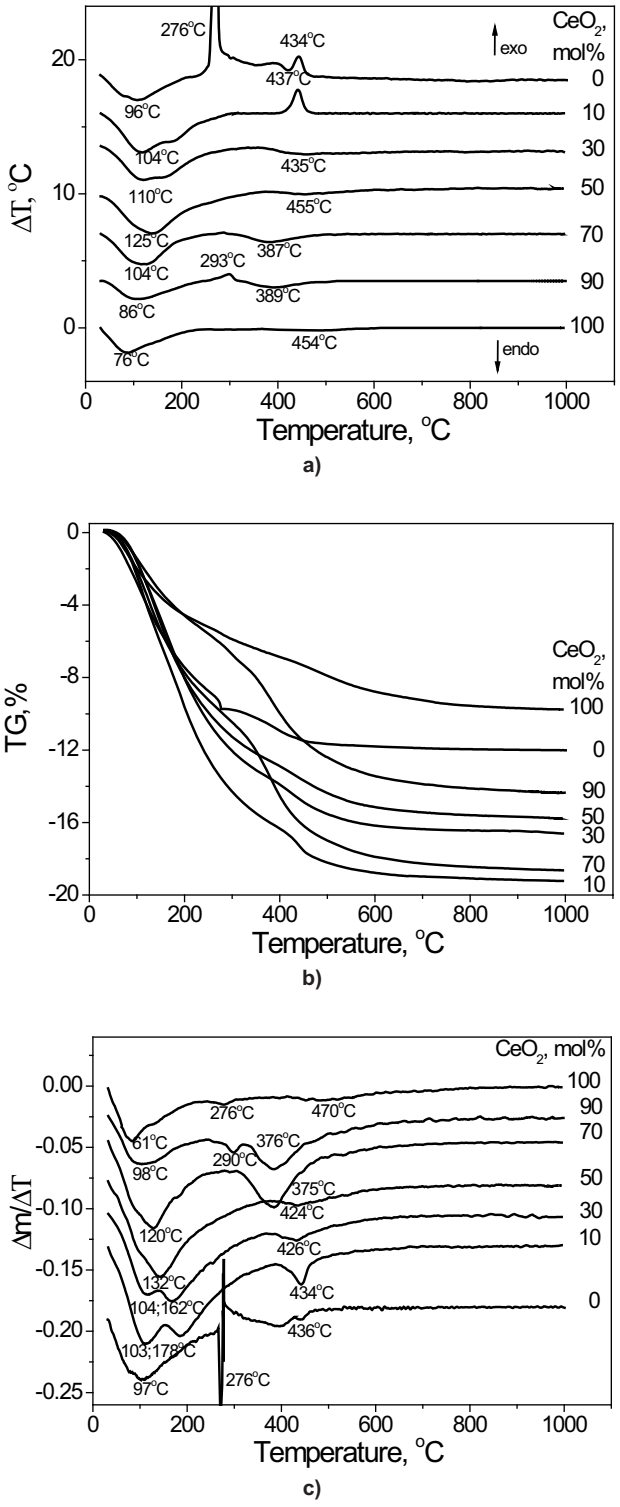

Fig. 2. Thermogravimetric analysis of co-precipitated deposits under air atmosphere at 10°C/min heating rate: a) DTA, b) TG, c) DTG.

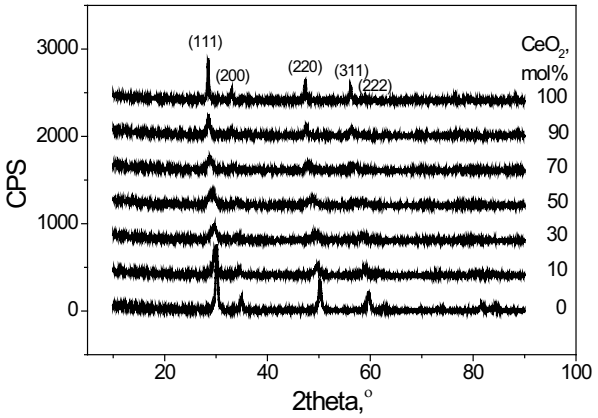

Fig. 3. X-ray diffraction patterns of the powders calcined for 1 h at 900°C in air.

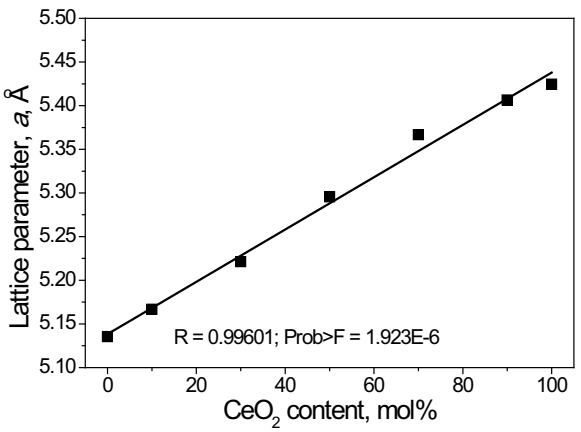

Fig. 4. Lattice parameter, a, of the powders calcined for 1 h at 900°C in air as a function of CeO_2 content.

effects are accompanied by the mass loss. The rate of mass loss corresponds well to the endothermic peaks, as shown by the DTG curves in Fig. 2c. The total mass loss shown by the materials with the ceria concentration from 50 to 90 % is larger than for pure ceria.

Based on the TG-DTA results, the deposits were calcined for 2 h at 900°C in air, and analysed by XRD before further processing. Fig. 3 shows X-ray diffraction patterns of the calcined deposits. All the powders crystallise in a face-centred cubic, fluorite type structure with space group Fm3m.

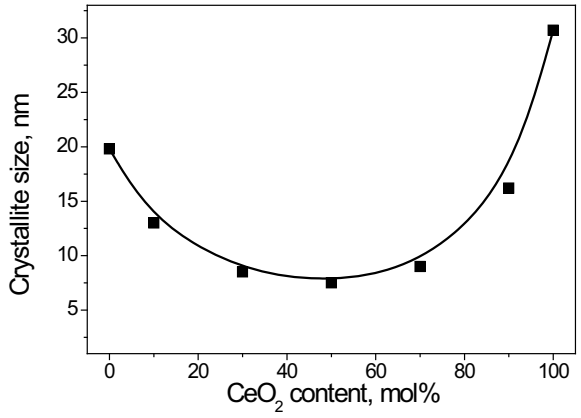

Fig. 5. Crystallite size of the powders calcined for 1 h at 900°C in air as a function of CeO_2 content.

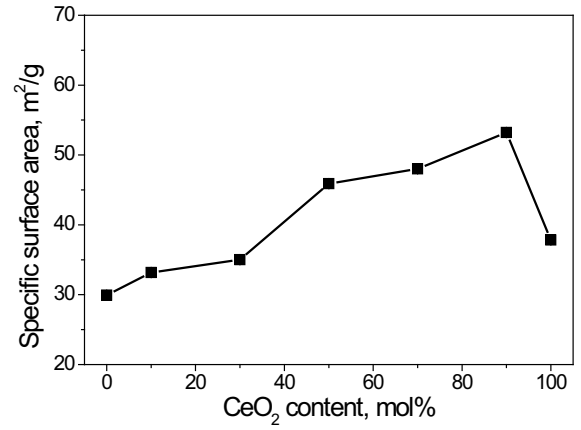

Fig. 6. Specific surface area of the powders calcined for 1 h at 900°C in air and milled for 2 h as a function of CeO_2 content.

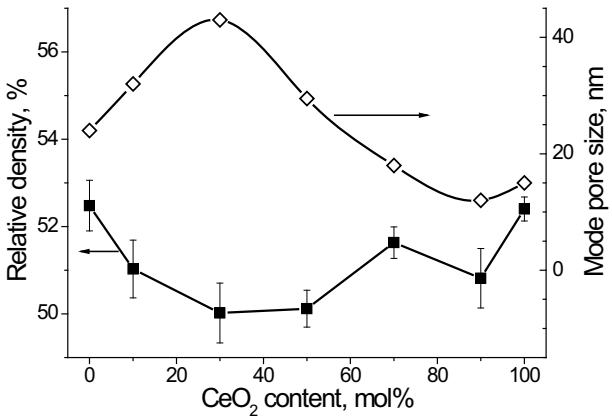

Fig. 7. Relative density and mode pore size of the green compacts originated from the studied powders as a function of CeO_2 content.

The lattice parameter of the calcined powders calculated from XRD patterns is plotted as a function of the ceria content in Fig. 4. The experimental data are well described by linear dependence (Vegard's law) with fit coefficients similar to 1:

$$a(\text{Å}) = 2.99 \cdot 10^{-3} \cdot C_{Ce} + 5.138;\ T_c = 900^{\circ}\text{C}, \qquad (1)$$

where C_{Ce} is the ceria concentration.

The experimental lattice parameters correlate with the data for respective solid solutions of ZrO_2 and CeO_2 from ICDD files [21, 22] and with the results presented in [6].

The synthesized materials containing from 10 to 90 mol% ceria are solid solutions with a composition corresponding

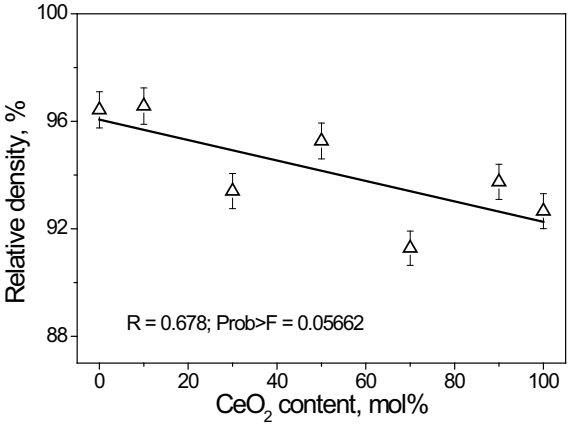

Fig. 8. Relative density of the materials sintered at 1550°C.

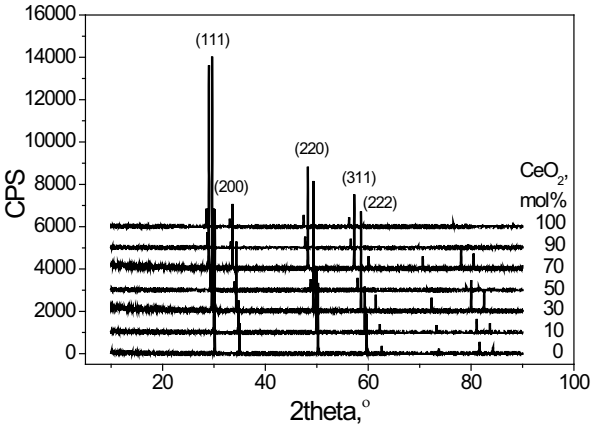

Fig. 9. Phase composition of the compacts sintered at 1550°C.

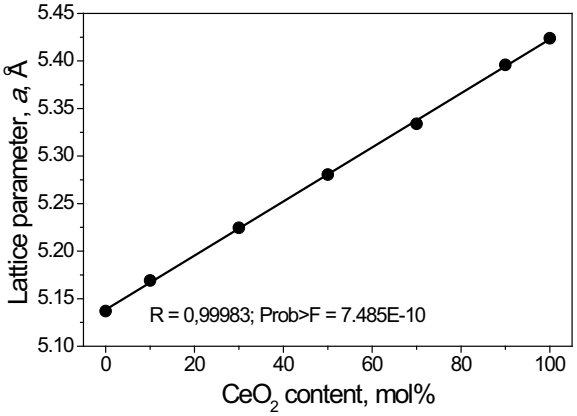

Fig. 10. Lattice parameter, a, as a function of CeO_2 content in the solid solutions measured for the materials sintered at 1550°C.

to the initial oxide contents, because their lattice parameters obey Vegard's law.

The microstructural development of the calcined powder was studied by estimating the crystallite size from X-ray line broadening by means of the Sherrer formula. The mean crystallite size as a function of ceria content is shown in Fig. 5. With increasing ceria content from 0 to 50 mol%, the crystallite size decreases from 19.8 to 7.5 nm, respectively, and then it increases up to 30.7 nm for the pure ceria. This result indicates that nucleation and growth of nuclei are strong functions of

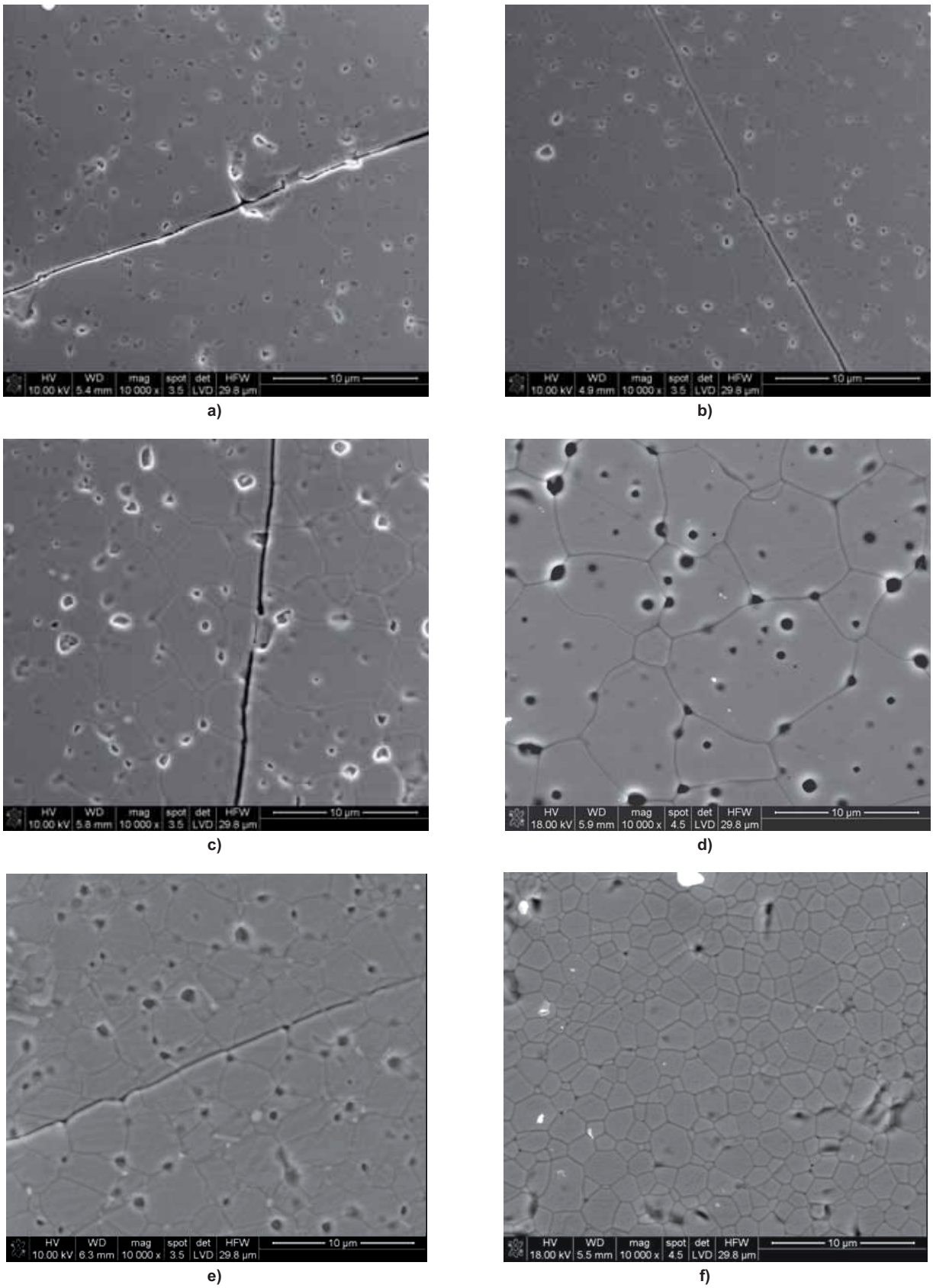

Fig. 11 SEM microphotographs of the compacts sintered at 1550°C in relation to CeO_2 content: a) 0 mol%, b) 10 mol%, c) 30 mol%, d) 50 mol%, e) 70 mol% and f) 100 mol%.

the ceria content in the studied powders. It is also evident that the formation of solid solution hinders the crystallite growth, favouring probably the nucleation process.

The specific surface area (S_w) of the powders after calcination at 900°C followed by 2 h milling given in Fig. 6 increases nearly linear in the range of ceria concentration from 0 to 90 mol%, starting from a value of 29.9 m^2/g and finishing on 53.2 m^2/g. For pure ceria, S_w abruptly decreases to 37.8 m^2/g. The specific surface area rather weakly correlates with the crystallite size, suggesting the presence of agglomerates of the nanocrystallites in the studied powders.

3.2. Green compacts and sinters

The behaviour of the calcined powders during compaction was investigated using porosimetry and the geometrical way of density evaluation. In Fig. 7, both the relative density and mode pore size of the compacts are plotted as a function of the ceria content in the powders. Densification of the compacts correlates well with the crystallite size according to a rule indicating that the larger crystallite size the larger density observed. Decreasing the crystallite size significantly inhibits densification of the compacts, and induces the prompt appearance of large pores. A slight increase in the pore size is detected for the compacts of pure ceria despite of the largest crystallites, suggesting the probable presence of hard agglomerates in the nanopowder.

The compacts were first naturally sintered at 1550°C in air, and then analysed by Archimedes' method and XRD. After sintering, a significant increase of density was observed, but full densification of the materials was not achieved, as shown in Fig. 8. Incorporation of ceria to the system generally decreased sinterability of the powders. Moreover, densification of the compacts was most probably affected by the fluctuation of powder morphology originated from powder processing, as suggested by a broad spread of the measured density values around the least square line (Fig. 8).

The ceria-zirconia-yttria solid solutions of a face-centred cubic (fcc) fluorite structure was detected in the sintered materials, as shown in Fig. 9. The results of the exact calculation of the lattice parameters are shown in Fig. 10. The experimental data are well described by a linear dependence (Vegards' law) and correlate with the data for respective solid solutions of ZrO_2 and CeO_2 from ICDD files [21, 22] and with the results presented in [6]:

$$a(Å) = 2.84 \cdot 10^{-3} \cdot C_{Ce} + 5.139;\ T_c = 1550°C \qquad (2)$$

In addition, the experimental data collected for sintered materials correlate with the literature data better, compared with those for the calcined powders. This is most probably a result of the crystallite size dependence of the experimental lattice parameter.

The microstructure evolution of ceria-zirconia-yttria sinters was investigated by SEM, and the results are shown in Figs. 11 and 12. The zirconia-yttria powders with different ceria content deliver the materials of microstructures, which differ in grain size, porosity and pore size. The grain size of the materials remains small and comparable in both the zirconia and ceria reach regions of the chemical composition (< 6.1 μm and < 3.9 μm, respectively), whilst the grains grow to a large extent (up to 13.6 μm) when a ratio of CeO_2 to ZrO_2 approaches the value of one (Fig. 12). In the latter case, the intra-grain pores are observed in a large content (Figs. 11c-e). For ceria concentrations lower than 30 %, the inter-grain pores dominate (Figs. 11a and 11b). However, for the ceria concentration higher than 70 %, the small amount of the inter-grain pores and the significant contribution of large voids appear. The forgoing results prove that the sintering behaviour of the ceria-zirconia-yttria nanopowders strongly depends on the ceria concentration.

Figs. 13 and 14 show the ceria concentration dependence of fracture toughness and hardness of the ceria-zirconia-ytt-

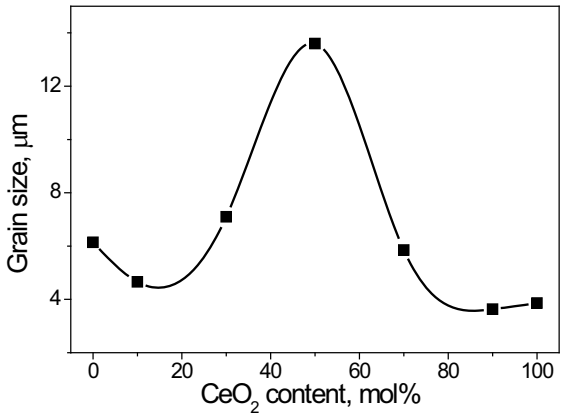

Fig. 12. Maximal grain size of materials sintered at 1550°C as a function of CeO_2 content.

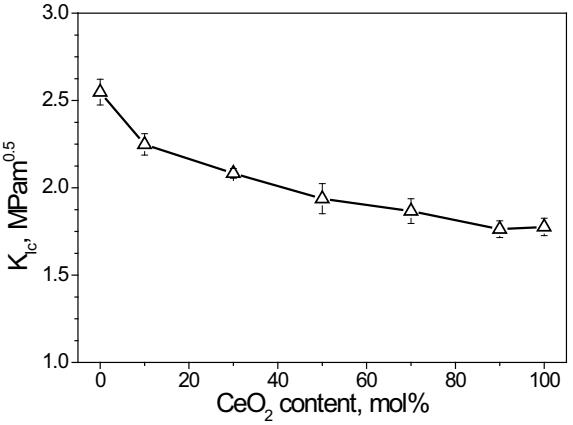

Fig. 13. Fracture toughness of the materials sintered at 1550°C as a function of CeO_2 content.

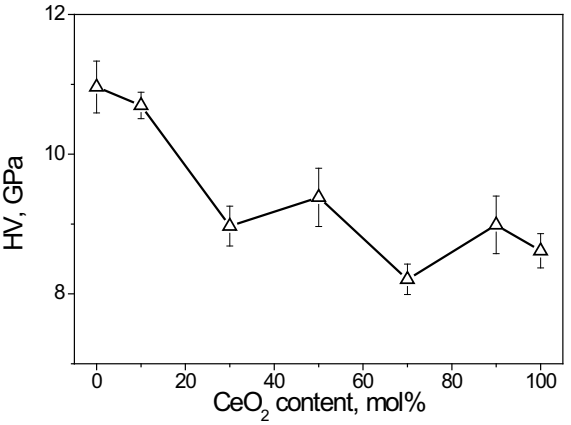

Fig. 14. Vickers' hardness of the materials sintered at 1550°C as a function of CeO_2 content.

tria materials, respectively. The continuous decrease of both toughness and hardness is observed, and it corresponds with the variation of composition and microstructure. The SEM investigations reveal the trans-granular fracture propagation during cracking (Fig. 11).

4. Conclusions

Ceria-zirconia-yttria nanopowders with the theoretical composition of $Y_{0.148}(Zr_{1-x}Ce_x)_{0.852}O_{2-\delta}$, where x = 0, 0.1, 0.3, 0.5, 0.7, 0.9 and 1.0, were manufactured by co-precipitation at room temperature followed by calcination. The nanopowders were naturally sintered to produce dense materials. The thermal behaviour of co-precipitated materials, crystal structure, evolution of the crystallite size, evolution of the microstructure and mechanical properties of the sintered materials were studied in detail using TG-DTA, XRD, BET, SEM and Vickers' indentation. It was shown that heat treatment of the co-precipitated material at 900°C leads to the nanocrystalline powders of ceria-zirconia yttria solid solutions with a face-centred cubic, fluorite type structure. The sintered materials showed the same crystal structure.

The lattice parameters of solid solutions detected in both the nanopowders and sintered materials were found to be a function of ceria content according to Vegard's low. Formation of the solid solution hindered the crystallite growth.

The behaviour of the nanopowders during both compaction and sintering was a function of ceria content according to the effect of ceria addition on the crystallite size.

The microstructure of the sintered materials was found to strongly depend on ceria content. For the ceria concentrations from 30 to 70 mol%, particularly intensive grain growth was found, accompanied by the formation of intra-grain pores in a large extent.

Fracture toughness and hardness decreased with ceria content according to its effects on the microstructure and densification. Hardness was affected strongly by porosity. Trans-granular cracking was found in the studied ceria-zirconia yttria materials.

Acknowledgements

This work was supported by the research fund of Polish Ministry of Science under the research-development project no. R 15 019 02. The authors would like to express their thanks to B. Trybalska from AGH-UST for performing the SEM observations.

References

[1] Ozawa M., Kimura M., Isogai A.: „The application of Ce–Zr oxide solid solution to oxygen storage promoters in automotive catalysts", J. Alloys Comp., 193, (1993),73-75.
[2] Sakai N., Xiong Y.P., Yamaji K., Kishimoto H., Horita T., Brito M.E., Yokokawa H.: „Transport properties of ceria–zirconia–yttria solid solutions $\{(CeO_2)_x(ZrO_2)_{1-x}\}_{1-y}(YO_{1.5})_y$ (x = 0–1, y = 0.2, 0.35)", J. Alloys Comp., 408-412, (2006), 503-506.
[3] Calès B., Baumard J.F.: „Mixed conduction and defect structure of ZrO_2-CeO_2-Y_2O_3 solid solutions", J. Electrochem. Soc., 131, (1984), 2407-2413.
[4] Arashi H., Naito H., Nakata M.: „Electrical-Properties in the ZrO_2–CeO_2–Y_2O_3 system", Solid State Ionics, 76, (1995) 315-319.
[5] Ananthapadmanabhan P.V., Venkatramani N., Rohatgi V.K., Momin A.C., Venkateswarlu K.S.: „Structure and ionic conductivity of solid solutions in the system $0.9\{(ZrO_2)_{1-x}$-$(CeO_2)_x\}$-$0.1(Y_2O_3)$", J. Eur. Ceram. Soc., 6, (1990), 111-117.
[6] Bukaemskiy A.A., Barrier D., Modolo G.: „Thermal and crystallization behaviour of 8YSZ-CeO_2 system", J. Alloys Comp., 472, (2009), 286-293.
[7] Oliveira A.P., Torem M.L.: „The influence of precipitation variables on zirconia powder synthesis", Powder Technol., 119, (2001), 181-193.
[8] Quinelato A.L., Longo E., Perazolli L.A., Varela J.A.: „Effect of ceria content on the sintering of ZrO_2 based ceramics synthesized from a polymeric precursor", J. Eur. Ceram. Soc., 20, (2000), 1077-1084.
[9] Aruna S.T., Patil K.C.: „Combustion synthesis and properties of nanostructured ceria-zirconia solid solutions", Nanostructured Mater., 10, (1998), 955-964.
[10] Dudek M., Mróz M., Zych Ł., Drożdż-Cieśla E.: „Synthesis of ceria-based nanopowders suitable for manufacturing solid oxide electrolytes", Mater. Sci. Poland, 26, (2008), 319-329.
[11] Shuk P., Greemblatt M.: „Hydrothermal synthesis and properties of mixed conductors based on $Ce_{1-x}Pr_xO_{2-\delta}$ solid solutions", Solid State Ionics, 116, (1999), 217-223.
[12] Li G., Smith R.L., Inomata H.: „Synthesis of nanoscale $Ce_{1-x}Fe_xO_2$ solid solutions via a low-temperature approach", J. Am. Chem. Soc., 123, (2001), 11091-11092.
[13] Singh P., Hegde M.S.: "Controlled synthesis of nanocrystalline CeO_2 and $Ce_{1-x}M_xO_{2-\delta}$ (M = Zr, Y, Ti, Pr and Fe) solid solutions by the hydrothermal method: Structure and oxygen storage capacity", J. Solid State Chem., 181, (2008), 3248-3256.
[14] Rietveld H.M.: „Line profiles of neutron powder-diffraction peaks for structure refinement", Acta Cryst., 22, (1967), 151-152.
[15] Scherrer P.: Göttinger Nachrichten Gesell., 2, (1918), 98-100.
[16] Niihara, K.A.: „A fracture mechanics analysis of indentation-induced Palmqvist crack in ceramics", J. Mater. Sci. Lett., 2, (1983), 221-223.
[17] Aronne A., Marotta A., Pernice P., Catauro M.: „Sol-gel processing and crystallization of yttria-doped zirconia", Therm. Acta, 275, (1996), 75-82.
[18] Guo G.Y., Chen Y.L., Ying W.J.: „Thermal, spectroscopic and X-ray diffractional analyses of zirconium hydroxides precipitated at low pH values", Mater. Chem. Phys., 84, (2004), 308-314.
[19] Caracoche M.C., Rivas P.C., Cervera M.M., Caruso R., Benavidez E., Sanctis O., Escobar M.E.: „Zirconium oxide structure prepared by the sol-gel route: I, The role of the alcoholic solvent", J. Am. Ceram. Soc., 83, (2000), 377-384.
[20] Haberko K.: „Characteristics and sintering behaviour of zirconia ultrafine powders", Ceramurgia Int., 5, (1979), 145-148.
[21] Powder Diffraction File No. 01-089-6687, International Centre for Diffraction Data, Newtown Square, PA.
[22] Powder Diffraction File No. 01-089-8436, International Centre for Diffraction Data. Newtown Square, PA.

♦

Received 1 March 2010: accepted 8 May 2010